Electromagnetic Remote Sensing Unveils Copious Sprites Currents Signatures During Two Consecutive Nights of Observations

Luis Contreras-Vidal[1], Richard Sonnefeld[2], Caitano da Silva[2], Matthew G. McHarg[3], Daniel Jensen[2], Jacob Harley[4], Lucie Taylor[5], Ryan K Haaland,[6], and Hans C. Stenbaek-Nielsen[7]

[1]New Mexico Institute of Mining and Technology
[2]New Mexico Tech
[3]United States Air Force Academy
[4]US Air Force Academy
[5]Fordham University
[6]Augsburg University
[7]University of Alaska Fairbanks

November 22, 2022

Abstract

On June 2nd and 3rd, 2019, 65 sprites were captured with a Phantom V2010 camera recording at 100,000 frames per second from Langmuir Laboratory (LL) in New Mexico. An extra sensitive slow-antenna known as LEFA, located 25 km east of LL, measured E-fields simultaneous with the video observations. Data from the Earth Networks Total Lightning Network (ENTLN) was used to locate their parent flash. By correlating all these datasets, we found the largest fraction of sprites with current signatures (45%) observed to date. These measured sprites have strong electromagnetic signatures comparable in magnitude to the largest current moments previously reported in the peer-reviewed literature, with range-normalized electric field changes of half the amplitude of their parent flashes, and current moments of up to 2742 kA km, as derived from a new computationally-efficient technique introduced here. Comparison to high-speed optical recordings shows also that optically-large sprites tend to have larger electrical currents.

Electromagnetic Remote Sensing Unveils Copious Sprites Currents Signatures During Two Consecutive Nights of Observations

L. Contreras-Vidal [1], R. Sonnenfeld [1], C. da Silva [1], M. McHarg [2], D. Jensen [1]J. Harley [2], L. Taylor [2], R. Haaland [3], H. Stenbaek-Nielsen [4]

[1]Department of Physics and Langmuir Laboratory, New Mexico Tech, Socorro, NM
[2]Department of Physics, U.S. Air Force Academy, Colorado Springs, CO
[3]Augsburg University, Minneapolis, MN
[4]University of Alaska Fairbanks, Geophysical Institute, Fairbanks, AK

Key Points:

- 65 sprites were detected using 100,000 fps high-speed video. VLF shows 45% of them have a sprite current signature
- New method to extract current moment was used to report remarkably large values up to 2742 kA km
- Optically-large sprites (carrots and jellyfish) tend to have larger electrical currents (median value is 33.8 kA)

Corresponding author: Luis Contreras-Vidal , luis.contrerasvidal@student.nmt.edu

Abstract

On June 2nd and 3rd, 2019, 65 sprites were captured with a Phantom V2010 camera recording at 100,000 frames per second from Langmuir Laboratory (LL) in New Mexico. An extra sensitive slow-antenna known as LEFA, located 25 km east of LL, measured E-fields simultaneous with the video observations. Data from the Earth Networks Total Lightning Network (ENTLN) was used to locate their parent flash. By correlating all these datasets, we found the largest fraction of sprites with current signatures (45%) observed to date. These measured sprites have strong electromagnetic signatures comparable in magnitude to the largest current moments previously reported in the peer-reviewed literature, with range-normalized electric field changes of half the amplitude of their parent flashes, and current moments of up to 2742 kA km, as derived from a new computationally-efficient technique introduced here. Comparison to high-speed optical recordings shows also that optically-large sprites tend to have larger electrical currents.

1 Introduction

Sprites consist of large scale electrical discharges taking place in the mesosphere, near the edge of space. They are triggered by quasi-electrostatic fields typically generated by positive cloud-to-ground lightning in underlying thunderstorms (Boccippio et al., 1995; da Silva & São Sabbas, 2013; Luque & Ebert, 2010; Pasko et al., 1997; Pasko, 2010). Since their discovery 30 years ago (Franz et al., 1990; Sentman et al., 1995), sprites have been extensively studied for their impact in mesospheric chemistry and their potential as a tool for remote sensing of the mesosphere-lower ionosphere interface, a region which is difficult to access by conventional observation techniques. In that time, researchers have remotely observed sprites' optical, electromagnetic (EM), and acoustic signatures. They have learned that certain sprites display an EM signature characteristic of a vertical current (Cummer, 2003; Pasko et al., 1998). However, measuring sprite currents remains challenging (Sonnenfeld & Hager, 2013).

Figure 1a shows an example of a Very Low Frequency (VLF) signature of one of the sprites we observed on June 3rd, 2019 and its parent flash. The return stroke pulse, detected by Earth Networks Total Lightning Network (ENTLN) and an extra sensitive antenna from the Langmuir Electric Field Array (LEFA), starts at $t = 0$. The second pulse at $t = 8.97$ ms is the EM signature of sprite currents.

Cummer et al. (1998) presented the first experimental evidence that current flowing in a sprite produces VLF radiation. They inferred the causal relationship between the sprite current signature and the sprite by showing that the peaks in the observed ELF waveforms occurring some milliseconds after the initial VLF sferic signal were coincident with the sprite's integrated optical brightness. Our Figure 1b shows the same clear relationship between optical signature and ELF waveform reported by Cummer et al. (1998). This unique feature allows for the detection of sprites from their radio signals without high speed video of the sprite. Stanley et al. (2000) reported the detection of 11 daytime sprites during a period of 3 days using the sprite current radio-signature.

EM signatures of sprite currents have been used for different quantitative and qualitative studies of sprites. Cummer and Stanley (1999) analyzed synchronized high speed video images and ELF-VLF radio emissions from 11 sprite clusters observed during October 6th, 1997. Their quantitative analysis showed that vertical lightning charge moment changes of 150−1100 C km occurred before the optical emissions reached their peak with delays of 2−11 ms from the lightning discharge. Years later, Cummer (2003) obtained maximum values of sprite current moment amplitudes of ∼1000 kA km from 76 sprites during a period of 17 days.

Hu et al. (2002) derived the charge moment of 76 observed sprite events from 17 days and presented an estimate of an average sprite current moment of ∼500 kA km. Li

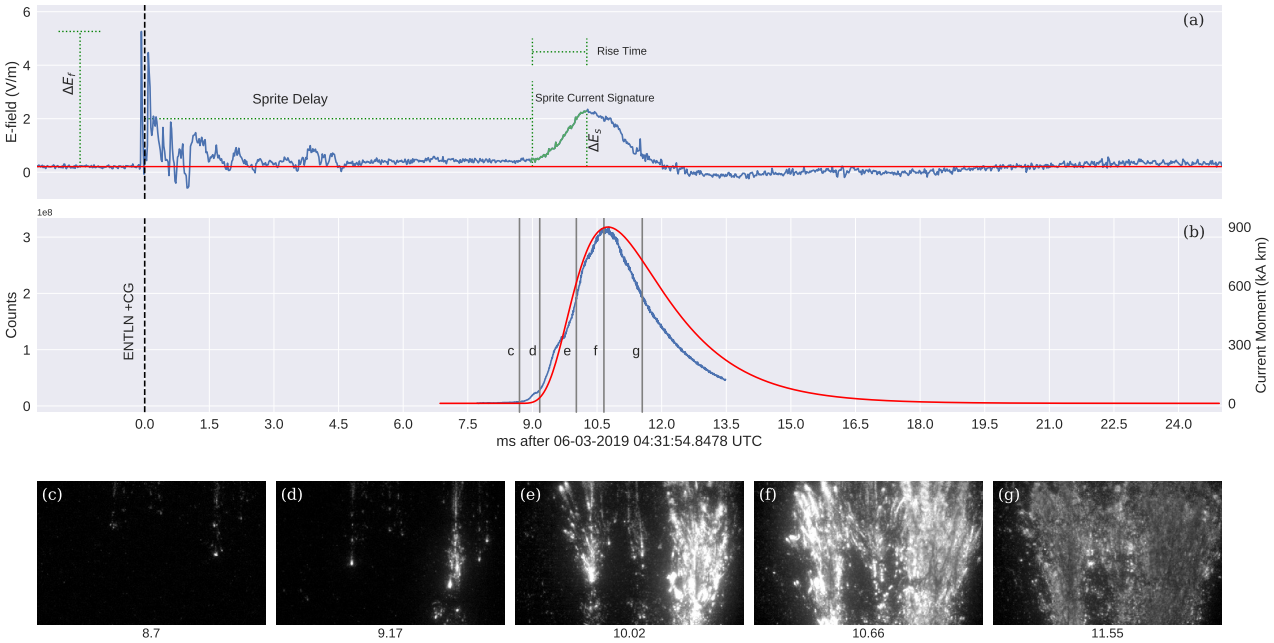

Figure 1. A sprite detected from Langmuir Lab in Central New Mexico, USA, on June 3, 2019. (a): E-field from parent flash and sprite. Black dashed line represents +CG detected by ENTLN. (b): Blue line represents high speed video integrated brightness. Red line corresponds to the extracted current moment for the sprite sferic (with magnitude shown in the right-hand side axis). (c-g) High speed video frames of the captured sprite. Frames are represented in panel (b) as vertical lines. Full video is available at https://doi.org/10.5281/zenodo.3875719

and Cummer (2011) estimated the electric charge moment of 4 sprites and reported sprite current moments of less than ∼400 kA km for two of them. Soula et al. (2015) reported that long-delayed sprites are associated with current moment waveforms of low amplitude and long duration. Gamerota et al. (2011) reported a maximum sprite current moment of ∼2750 kA km, the highest value we found in the peer-reviewed literature. Sonnenfeld and Hager (2013) used electric field data from a sprite to model the electric field associated with its current, estimating the sprite peak current to be 18 kA.

In this study, we present a physical characterization and statistical analysis of optical and E-field measurements of 65 sprites and their parent flashes. These sprites were observed during the nights of June 2 and 3, 2019 at the Langmuir Laboratory for Atmospheric Research located in central New Mexico (34.06 N, 106.90 W) and account for the largest sprite current dataset ever reported. We also present an empirical measurement of the sprite currents as would be estimated by a lightning detection network, a statistical measure of sprite delays, calculations of current moment from sprite sferics, a comparison between the measured sferics and electromagnetic simulations, and a description of the relation between the sprite current moment and their morphology.

2 Instruments and Datasets

The EM signature in Figure 1a was recorded with one of the extra sensitive slow antennas from Langmuir Lab's LEFA array. The three-channel design of the LEFA slow antenna extends the dynamic range of electrostatic field change measurements from 0.021 V/m to 496 kV/m. The data-acquisition-module is set to 50 kS/s sustained sampling

rate, which covers the range of time-scales of the electrostatic processes in lightning (Zhang, 2010; Hager et al., 2012). Calibration of LEFA is described in detail by Hager et al. (2012). Because calibration of electric field instruments is very sensitive to the elevation and morphology of the deployment site, the electric fields quoted here are accurate to only ±15% (1 σ).

Classification, location, peak current and timing of the parent flashes were obtained from the ENTLN. ENTLN is a global lighting detection network that has been operational since 2009. The ENTLN sensors are broadband electric field sensors that detect both intra-cloud (IC) and cloud-to-ground (CG) lightning with high efficiency and provide accurate timing, location, classification, and peak current measurements. It consists of over 1600 wideband sensors deployed in 40+ countries to detect lightning and generate faster-localized storm alerts (Lapierre, 2019). Evaluation of ENTLN performance results have shown a total flash detection efficiency of 97.5% and classification accuracy of of 91% for CG flashes (Lapierre, 2019). The median values of location error and absolute peak current estimation error of ENTLN have been reported to be 215 m and 15% respectively by using cloud-to-ground (CG) lightning data acquired at the Lightning Observatory in Gainesville as ground truth and rocket-triggered lightning data obtained at Camp Blanding, Florida (Zhu et al., 2017).

A 4-megapixel Phantom V2640 high-speed video camera operating at up to 100,000 frames per second, is used to produce the "ground truth" light curves, such as the one shown in Figure 1b. The camera also allows morphological classification of the detected sprites. The Phantom camera recorded sprites as far as 800 km from Langmuir Lab. The high-speed video captured (Figures 1c to 1g) showed streamers starting to move downward 8.7 ms after the parent flash (frame c). At 9.17 ms (frame d), the Phantom v2640 recorded that the sprite element on the right increased brightness and that a second sprite element has been initiated on the left-hand side of the frame. After 10.02 ms (frame e), three sprite carrots can be identified in the field of view, with clear upward streamer development, along with an overall increase in sprite brightness. Peak brightness was reached at 10.66 ms after its parent flash (frame f), followed by uniform decay in luminosity (frame g).

3 Methodology

Every ENTLN positive cloud-to-ground (CG) flash in a radius of 100 km from the observed storm was synchronized with LEFA data and integrated optical brightness from the high speed video (Figure 1). Both LEFA data and integrated optical brightness have been corrected to transmission delays. Through LEFA, we were able to quantify some characteristics of the radiated electromagnetic field, such as the electric field change of the parent flash (ΔE_f), the electric field change of the sprite (ΔE_s), the 10–90% rise-time of characteristic sprite signature, and the delay of the sprite signature. The electric field changes are measured with respect to the average electric field value in a 2.5-ms window preceding the parent flash, and the sprite delay is measured with respect to the ENTLN-reported time of the parent flash. We accepted the peak current of the parent flash as reported by ENTLN. Figure 1a illustrates how these waveform features are defined.

On June 2, 363 CG flashes between 03:00 and 08:00 UTC located near the border of Texas and Oklahoma were analyzed. Fifteen flashes showed a characteristic sprite signature which aligned with high speed video integrated brightness. Nine flashes aligned with high speed video but no characteristic sprite signature was observed. These CG flashes were located at an average distance of 689 km from Langmuir Lab (Figure 2a).

On the following night of June 3, 113 CG flashes between 04:00 and 06:10 UTC located on northwest Texas were analyzed. Fourteen flashes showed a characteristic sprite

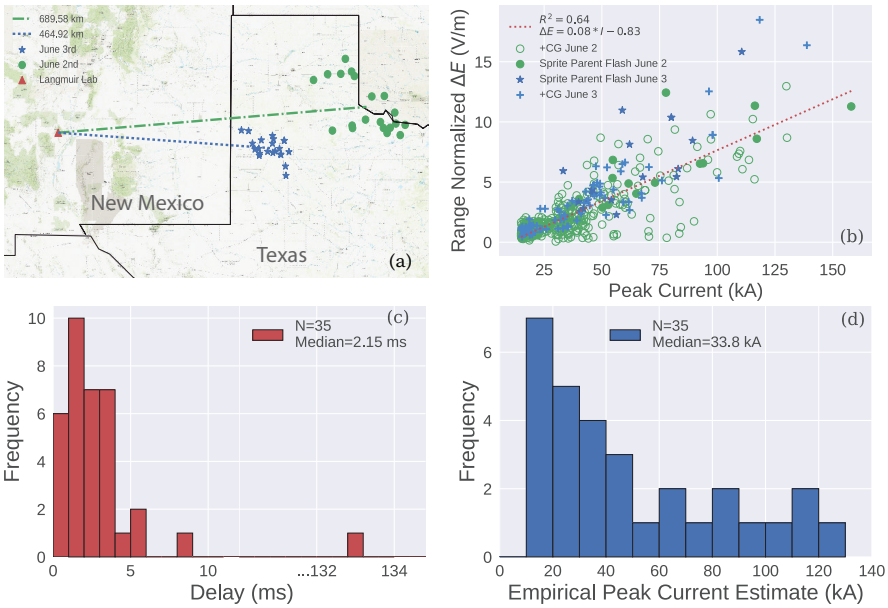

Figure 2. (a) Map shows the location of the parent flashes detected by ENTLN during both nights. (b) Range-normalized ΔE_f of flash vs ENTLN peak current (c) Sprite delay distribution histogram. The median sprite delay is 2.15 ms. (d) Sprite currents distribution. The median sprite current is 11.3 kA

signature which aligned with high speed video integrated brightness. Seven other flashes aligned with peak integrated optical brightness but no characteristic sprite signature was observed. These +CGs flashes were located at an average distance of 465 km from Langmuir Lab (Figure 2a).

The vertical electric field just above the surface of a perfectly-conducting ground, at plane distance D from the source, can be conveniently expressed as a sum of three components, derived from an integral solution to the Maxwell's equations:

$$E(t) = \sum_{i=1}^{N} \frac{s_I^{i+1}}{2\pi\varepsilon_0} \left\{ \frac{(2-3\sin^2\theta_i)}{R_i^3} M_Q(t_i') + \frac{(2-3\sin^2\theta_i)}{cR_i^2} M_I(t_i') - \frac{\sin^2\theta_i}{c^2 R_i} \frac{dM_I(t_i')}{dt} \right\} \quad (1)$$

where M_Q is the charge moment change, $M_I = dM_Q/dt$ is the current moment, $R_i = \sqrt{h_i^2 + D^2}$ is the source-observer distance, $\sin\theta_i = D/R_i$, $t_i' = t - R_i/c$ is the retarded time, s_I indicates the direction (or sign) of current propagation ($+1 =$ upward, $-1 =$ downward), ε_0 is the vacuum electric permittivity, and c is the speed of light. For a distributed source current $I(z,t)$, as function of height z and time t, the current moment can be obtained as $M_I(t) = \int I(z,t)dz$.

If we reduce the summation above to a single term ($N = 1$), equation (1) describes the electric field produced by a source at height h_1 above a perfectly-conducting ground plane and its image. This equation is a simplification of Uman's derivation, commonly used for simulation of lightning electromagnetic fields (Uman et al., 1975) if the source is small in comparison to source-observer distance (da Silva & Pasko, 2015, equations

(7)-(10)). The three terms inside the curly brackets are commonly referred to as electrostatic, induction, and radiation components of the total electric field, respectively. For distances far away from the source the radiation term dominates because of its weaker dependence on the source-observer distance. For this reason, the electric field changes reported here are range-normalized by a $D_{\rm n}/D$ factor, as it is common practice for lightning detection systems (Orville, 1991). We use here $D_{\rm n} = 500$ km. Extending equation (1) to an infinite summation ($N \to \infty$), allows one to account for the effects of image sources in the ionosphere (Hager et al., 2012), modeled as a perfect conductor at a height H above ground. This is done by realizing that every ionospheric image produces a subsequent image on the ground and so on. The effective source heights for these image currents are $h_i = iH - h_1$ if i is even or $h_i = (i-1)H + h_1$ if i is odd (Hager et al., 2012; Sonnenfeld & Hager, 2013).

In this study, we use equation (1) to retrieve the sprite current moments. The current moment is produced by a current pulse propagating downward from 80 to 70 km altitude at a speed of 10^7 m/s. The current pulse shape is described by a Heidler (1985) function, and its amplitude varies as a function of distance according to a smooth Gaussian function (da Silva et al., 2016, equation (7)). The current pulse risetime and falltime are empirically adjusted to fit the recorded sprite sferic. The approach is validated by comparison with the full solution obtained from a two-dimensional FDTD simulation code (Marshall, 2012; Marshall et al., 2015). The FDTD simulations are made in spherical coordinates, accounting for Earth's curvature. The ground is represented as a perfect conductor, and the ionosphere is represented as a cold plasma according to a Wait and Spies (1964) electron density profile suitable for the nighttime ionosphere at mid-latitudes.

4 Results

During the two observation nights we detected 65 sprites. Twenty nine of them had a sprite current signature (45%). Cummer (2003) previously reported a fraction of 10% sprite current signatures based on Extreme Low Frequencies (ELF) radiation observations (Cummer et al., 2006). We have also detected 6 additional sprites exclusively by their EM signature, with no associated video record, similarly to Stanley et al. (2000). The median risetime of the detected sprite electric field signatures is 1.09 with a standard deviation of 0.45 ms.

Figure 2b shows the range normalized ΔE_f vs peak current (I_p) for all the +CGs for both nights. The electric field has been normalized by D/D_n, where D is the distance of the flash from Langmuir Lab and $D_n = 500$ km. The coefficient of determination is $R^2 = 0.64$ of the linear fit shown in Figure 2b. The average peak current of sprite-parent flashes is 69.3 kA. In addition, the average values for ΔE_f and ΔE_s are 6.79 and 3.08 V/m respectively, making ΔE_s nearly half of ΔE_f.

Sprite delays were obtained and compared to previous literature. Figure 2c shows our distribution of sprite delays. Most of the observed sprites have short delays ranging between 0.14 and 8.97 ms, with a median value of 2.15 ms. Typical delays have been reported before to be less than 5 ms (Li et al., 2008). Long-delayed sprites are defined as sprites that initiates more than 10 ms after a return stroke (Li et al., 2008), such as the sprite with a delay of 132.8 ms in Figure 2c. Li et al. (2008) has reported long delayed sprites ranging from 10 ms to 290 ms.

Repurposing the linear fit derived in Figure 2b: $I_p = (\Delta E_s + 0.83)/0.08$, with ΔE_s being the electric field change of the sprite and I_p in units of kA; we obtained a distribution of empirically-determined sprite currents, as if measured by a lightning detection network (Figure 2d). The estimate assumes that the peak current is simply proportional to the range-normalized electric field change, with no correction to the size of the

electromagnetic radiator; this method is tested in the subsequent paragraphs using electromagnetic simulations. The minimum and maximum values of the sprite currents calculated here are 17.4 and 121.8 kA, while the median value is 33.8 kA. As a comparison point, Cummer (2003) estimate values of the order of 25 kA.

Figure 1b shows the extracted current moment for the sprite sferic shown in Figure 1a using equation (1). Figure 3a shows a comparison between measured and simulate electric field change waveforms. The quality of fit is ensured by a high value for the coefficient of determination between simulation and data, $R^2 = 0.982$. Figure 3a shows not only that the analytical solution can match the observations, but that it is also virtually equivalent to the result yielded by a FDTD simulation accounting for Earth's curvature (Marshall, 2012). Figure 3b shows the contributions of the three terms between the curly brackets in equation (1) to the total electric field, illustrating that although the radiation component is dominant, the other two components are significant. In fact, our simulations indicate that the current moment shown in Figure 1b produces an electric field change that varies with distance as $1/D^{0.46}$ for distances between 300 and 600 km.

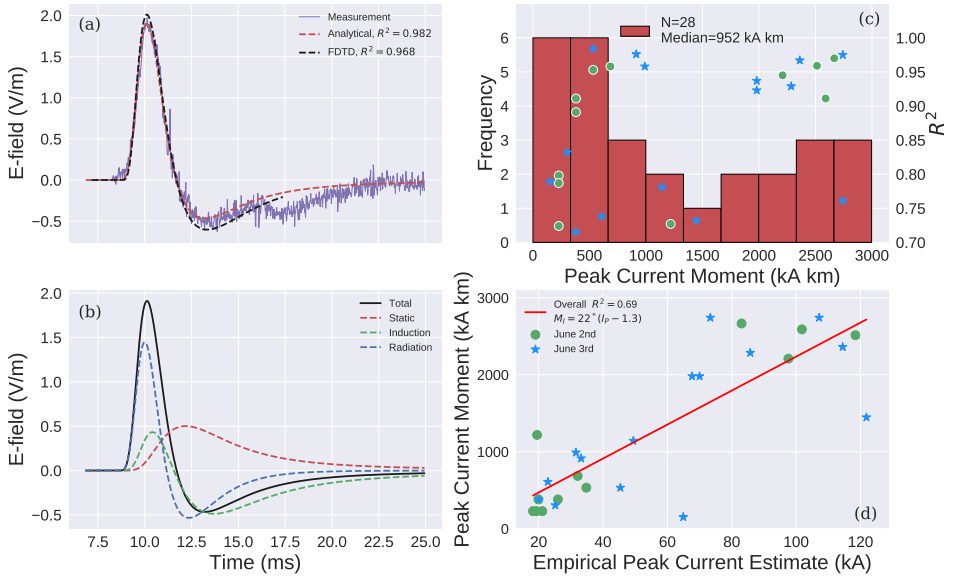

Figure 3. (a) Comparison between measured sferic, simulated with equation (1), and simulated via the FDTD technique. (b) The static, induction, and radiation components of the total electric field. (c) Right-axis shows the coefficient of determination used as a quality-of-fit metric for the distribution of peak currents plotted on the left y-axis. The R^2 is calculated from panel (a). (d) Relation between the calculated peak current moment of the sprites and their empirical peak current moment estimate.

Figure 3c shows the distribution of peak current moments extracted from the 28 waveforms for which a good fit between simulation and measurement could be obtained, i.e., for $R^2 > 0.7$, as shown in the right-hand side vertical axis. The median peak current moment inferred here is 952 kA km, while the maximum is 2742 kA km, which compares in magnitude to the highest value previously reported in the peer-reviewed liter-

ature ∼2750 kA km (Gamerota et al., 2011). This distribution of peak current moments is different than the distribution of peak currents seen in Figure 2d (which is equivalent to the distribution of range-normalized electric field changes), the distribution of peak current moments does not decrease monotonically, it actually has a secondary peak at 2750 kA km. The fact that all fits yielding values >2500 kA km are obtained with a high-level of accuracy (all with $R^2 > 0.9$, with the exception of only one with $R^2 > 0.75$), gives us confidence to state that the sprite signatures reported here correspond to some of the strongest sprite current moments ever measured. The quantity current moment is preferred here (instead of simply current) because it is not affected by the ambiguities involved in evaluating the electric field radiated by a source that is small in comparison to its distance to the observed (da Silva et al., 2016).

Figure 3d shows the relation between the calculated peak current moment of the sprites and their empirical peak current estimate. The linear relation $M_I = 22 \cdot (I_p - 1.3)$ indicates that peak current estimates are approximately valid under the assumption that the sprite EM radiator has 22 km of length. But more importantly, the figure shows that the two quantities are not precisely linearly proportional ($R^2 = 0.69$), demonstrating the need to precisely fit the electric change waveform when estimating the source current parameters, and making the peak current estimates in Figure 2d not precisely accurate. The discrepancy happens largely because the two types of electric field change waveforms (flash versus sprite) have very different risetimes, and also due to effects of ionospheric images.

Our results indicate that sprites with stronger peak current moments are bigger and have more complicated morphologies, or more precisely we can state that: (i) Five sprites with peak current moment less than 230 kA km and five with no signature at all are of the columniform type, (ii) the nine sprites with peak current moment larger than 1980 kA km are classified as of the carrot or jellyfish type, (iii) the two jellyfish sprites are within the top three peak current moments, and (iv) in the intermediate range between 230 and 1980 kA km, all types of morphologies can be detected. Our findings further the idea that large and vigorously-luminous sprites have stronger currents, therefore making these easily-identifiable optical characteristics a proxy for the energetic impacts of sprites in the mesosphere (da Silva & Pasko, 2014; Sentman et al., 2008).

Cummer (2003) notes that upward streamers are associated only to events with sprite current signatures. Here, we find that column sprites consisting of only downward streamer may present current signatures, but that they tend to be substantially weaker than in carrot sprites that contain upward streamer development. In Figure 1b, we see that the current moment growth correlates with the sprite optical growth, mostly due to streamer expansion and branching, both down and upward. The peak current moment happens roughly at the same time as peak brightness, dominated by the luminosity of glowing structures inside existing streamer channels. This is in agreement with Cummer et al. (2006), who stated that sprite current flows most strongly during subsequent brightening of the sprite, and not during initial downward streamer motion. The uniform luminosity decay shown in Figure 1g, correlated with the current moment reduction, is in alignment with the conclusions of Luque et al. (2016) that distant points within a channel decay at the same rate despite considerable differences in the underlying air density and electronic conductivity.

5 Summary

In this study, we have reported a large number of electromagnetic sprite current signatures obtained in just two consecutive nights of observations. In this dataset, we've found the largest fraction of detected sprites with current signature reported to date, amounting 45%, substantially larger than the 10% found in the literature. Moreover, the sprite currents registered in this study are some of the strongest ever reported, with range-normalized

electric field changes that have around half the amplitude of its parent flash's, amounting to peak current moments of up to 2742 kA km, as estimated from a new computationally-efficient extraction technique introduced in this paper. Optically-large sprites tend to produce larger electrical currents, and thus deposit more energy in the mesosphere. Future research will involve determining whether intense sprite currents are a common feature from storms in North Texas, and what would be the potential reason. Further research will also help clarify the relationship between sprite current and the interplay of intricate streamer dynamics and the longer lasting sprite glows and beads.

Acknowledgments

This work has been supported by the NSF EPSCoR Program under award OIA-1757207, by NSF award AGS-1917069, and by collaborative grants from Vaisala and Earth Networks. We also thank Earth Networks for making ENTLN pulse data readily available. Data is publicly available at https://doi.org/10.5281/zenodo.3875719.

References

Boccippio, D. J., Williams, E. R., Heckman, S. J., Lyons, W. A., Baker, I. T., & Boldi, R. (1995). Sprites, ELF transients, and positive ground strokes. *Science*, *269*, 1088–1091. doi: 10.1126/science.269.5227.1088

Cummer, S. A. (2003). Current moment in sprite-producing lightning. *Journal of Atmospheric and Solar-Terrestrial Physics*, *65*(5), 499 - 508. Retrieved from `http://www.sciencedirect.com/science/article/pii/S1364682602003188` (Sprites, Elves and their Global Activities) doi: https://doi.org/10.1016/S1364-6826(02)00318-8

Cummer, S. A., Frey, H. U., Mende, S. B., Hsu, R.-R., Su, H.-T., Chen, A. B., ... Takahashi, Y. (2006). Simultaneous radio and satellite optical measurements of high-altitude sprite current and lightning continuing current. *Journal of Geophysical Research: Space Physics*, *111*(A10). Retrieved from `https://agupubs.onlinelibrary.wiley.com/doi/abs/10.1029/2006JA011809` doi: 10.1029/2006JA011809

Cummer, S. A., Inan, U. S., Bell, T. F., & Barrington-Leigh, C. P. (1998). Elf radiation produced by electrical currents in sprites. *Geophysical Research Letters*, *25*(8), 1281-1284. Retrieved from `https://agupubs.onlinelibrary.wiley.com/doi/abs/10.1029/98GL50937` doi: 10.1029/98GL50937

Cummer, S. A., & Stanley, M. (1999). Submillisecond resolution lightning currents and sprite development: Observations and implications. *Geophysical Research Letters*, *26*(20), 3205-3208. Retrieved from `https://agupubs.onlinelibrary.wiley.com/doi/abs/10.1029/1999GL003635` doi: 10.1029/1999GL003635

da Silva, C. L., Merrill, R. A., & Pasko, V. P. (2016). Mathematical constraints on the use of transmission line models to investigate the preliminary breakdown stage of lightning flashes. *Radio Sci.*, *51*(5), 367–380. doi: 10.1002/2015RS005853

da Silva, C. L., & Pasko, V. P. (2014). Infrasonic acoustic waves generated by fast air heating in sprite cores. *Geophys. Res. Lett.*, *41*(5), 1789–1795. doi: 10.1002/2013GL059164

da Silva, C. L., & Pasko, V. P. (2015). Physical mechanism of initial breakdown pulses and narrow bipolar events in lightning discharges. *J. Geophys. Res.*, *120*(10), 4989–5009. doi: 10.1002/2015JD023209

da Silva, C. L., & São Sabbas, F. T. (2013). Consequences of the application of the streamer fluid model to the study of the sprite inception mechanism. *Adv. Space Res.*, *51*(10), 1902–1915. doi: 10.1016/j.asr.2012.11.025

Franz, R. C., Nemzek, R. J., & Winckler, J. R. (1990). Television image of a large upward electrical discharge above a thunderstorm system. *Science*, *249*, 448–

451. doi: 10.1126/science.249.4964.48

Gamerota, W. R., Cummer, S. A., Li, J., Stenbaek-Nielsen, H. C., Haaland, R. K., & McHarg, M. G. (2011). Comparison of sprite initiation altitudes between observations and models. *Journal of Geophysical Research: Space Physics*, *116*(A2). Retrieved from https://agupubs.onlinelibrary.wiley.com/doi/abs/10.1029/2010JA016095 doi: 10.1029/2010JA016095

Hager, W. W., Sonnenfeld, R. G., Feng, W., Kanmae, T., Stenbaek-Nielsen, H. C., McHarg, M. G., ... Lapierre, J. L. (2012). Charge rearrangement by sprites over a north Texas mesoscale convective system. *J. Geophys. Res.*, *117*. doi: 10.1029/2012JD018309

Heidler, F. (1985). Traveling current source model for LEMP calculation. In *Proc. 6th int. zurich symp. electromagnetic compatibility* (pp. 157–162). Zurich, Switzerland.

Hu, W., Cummer, S. A., Lyons, W. A., & Nelson, T. E. (2002). Lightning charge moment changes for the initiation of sprites. *Geophysical Research Letters*, *29*(8), 120-1-120-4. Retrieved from https://agupubs.onlinelibrary.wiley.com/doi/abs/10.1029/2001GL014593 doi: 10.1029/2001GL014593

Lapierre, J. (2019). Earth networks lightning performance in: International conference on lightning and static electricity. Wichita, Kansas, USA.

Li, J., & Cummer, S. (2011). Estimation of electric charge in sprites from optical and radio observations. *Journal of Geophysical Research: Space Physics*, *116*(A1). Retrieved from https://agupubs.onlinelibrary.wiley.com/doi/abs/10.1029/2010JA015391 doi: 10.1029/2010JA015391

Li, J., Cummer, S. A., Lyons, W. A., & Nelson, T. E. (2008). Coordinated analysis of delayed sprites with high-speed images and remote electromagnetic fields. *Journal of Geophysical Research: Atmospheres*, *113*(D20). Retrieved from https://agupubs.onlinelibrary.wiley.com/doi/abs/10.1029/2008JD010008 doi: 10.1029/2008JD010008

Luque, A., & Ebert, U. (2010). Sprites in varying air density: Charge conservation, glowing negative trails and changing velocity. *Geophys. Res. Lett.*, *37*. doi: 10.1029/2009GL041982

Luque, A., Stenbaek-Nielsen, H. C., McHarg, M. G., & Haaland, R. K. (2016). Sprite beads and glows arising from the attachment instability in streamer channels. *Journal of Geophysical Research: Space Physics*, *121*(3), 2431-2449. Retrieved from https://agupubs.onlinelibrary.wiley.com/doi/abs/10.1002/2015JA022234 doi: 10.1002/2015JA022234

Marshall, R. A. (2012). An improved model of the lightning electromagnetic field interaction with the D-region ionosphere. *J. Geophys. Res.*, *117*. doi: 10.1029/2011JA017408

Marshall, R. A., da Silva, C. L., & Pasko, V. P. (2015). Elve doublets and compact intracloud discharges. *Geophys. Res. Lett.*, *42*(14), 6112–6119. doi: 10.1002/2015GL064862

Orville, R. E. (1991). Calibration of a magnetic direction finding network using measured triggered lightning return stroke peak currents. *J. Geophys. Res.*, *96*(D9), 17135–17142. doi: 10.1029/91JD00611

Pasko, V. P. (2010). Recent advances in theory of transient luminous events. *J. Geophys. Res.*, *115*. doi: 10.1029/2009JA014860

Pasko, V. P., Inan, U. S., Bell, T. F., & Reising, S. C. (1998). Mechanism of ELF radiation from sprites. *Geophys. Res. Lett.*, *25*(18), 3493–3496. doi: 10.1029/98GL02631

Pasko, V. P., Inan, U. S., Bell, T. F., & Taranenko, Y. N. (1997). Sprites produced by quasi-electrostatic heating and ionization in the lower ionosphere. *J. Geophys. Res.*, *102*(A3), 4529–4561. doi: 10.1029/96JA03528

Sentman, D. D., Stenbaek-Nielsen, H. C., McHarg, M. G., & Morrill, J. S. (2008). Plasma chemistry of sprite streamers. *J. Geophys. Res.*, *113*. doi: 10.1029/

2007JD008941

Sentman, D. D., Wescott, E. M., Osborne, D. L., Hampton, D. L., & Heavner, M. J. (1995). Preliminary results from the Sprites94 aircraft campaign: 1. Red sprites. *Geophys. Res. Lett.*, *22*(10), 1205–1208. doi: 10.1029/95GL00583

Sonnenfeld, R. G., & Hager, W. W. (2013). Electric field reversal in sprite electric field signature. *Mon. Weather Rev.*, *141*, 1731–1735. doi: 10.1175/MWR-D-12-00220.1

Soula, S., Defer, E., Füllekrug, M., van der Velde, O., Montanya, J., Bousquet, O., ... Pedeboy, S. (2015). Time and space correlation between sprites and their parent lightning flashes for a thunderstorm observed during the hymex campaign. *Journal of Geophysical Research: Atmospheres*, *120*(22), 11,552-11,574. Retrieved from `https://agupubs.onlinelibrary.wiley.com/doi/abs/10.1002/2015JD023894` doi: 10.1002/2015JD023894

Stanley, M., Brook, M., Krehbiel, P., & Cummer, S. A. (2000). Detection of daytime sprites via a unique sprite elf signature. *Geophysical Research Letters*, *27*(6), 871-874. Retrieved from `https://agupubs.onlinelibrary.wiley.com/doi/abs/10.1029/1999GL010769` doi: 10.1029/1999GL010769

Uman, M. A., McLain, D. K., & Krider, E. P. (1975). The electromagnetic radiation from a finite antenna. *Am. J. Phys.*, *43*(1), 33–38. doi: 10.1119/1.10027

Wait, J. R., & Spies, K. P. (1964). *Characteristics of the Earth-ionosphere waveguide for VLF radio waves* (Vol. 13; Tech. Rep. No. 300). Natl. Bur. of Stand., Boulder, Co.

Zhang, J. (2010). Development and test of the langmuir electric field array master's. *Thesis. New Mexico Institue of Mining and Technology*.

Zhu, Y., Rakov, V. A., Tran, M. D., Stock, M. G., Heckman, S., Liu, C., ... Hare, B. M. (2017). Evaluation of entln performance characteristics based on the ground truth natural and rocket-triggered lightning data acquired in florida. *Journal of Geophysical Research: Atmospheres*, *122*(18), 9858-9866. Retrieved from `https://agupubs.onlinelibrary.wiley.com/doi/abs/10.1002/2017JD027270` doi: 10.1002/2017JD027270